

PAPER

[View Article Online](#)
[View Journal](#) | [View Issue](#)Cite this: *J. Mater. Chem. A*, 2023, 11, 20559

Delivering low-energy carbon capture with photo-responsive hypercrosslinked polymers derived from polystyrene waste†

Aotian Liu,‡ Guanchu Lu,‡ Xianfeng Fan* and Cher Hon Lau *

Highly effective but energy-intensive techniques such as temperature and pressure swing adsorption are typically deployed to regenerate adsorbents used in carbon capture. Here we show that the energy consumption and costs associated with adsorbent regeneration can be reduced by 500-fold when photo-responsive hypercrosslinked polymers (HCPs) recycled from waste expanded polystyrene that are loaded with 8.9 wt% of azobenzene are deployed for carbon capture. Our approach uses UV light (365 nm) to enhance the adsorption of CO₂ from a variety of mixed gas concentrations with CO₂ content between 1–40 v/v%. 14% of CO₂ adsorbed on HCPs@Azo can be desorbed by irradiation with visible light. The photo-regeneration efficiency of adsorption and desorption capacities of HCPs@Azo stabilised at 50% after 5 cycles, demonstrating good reusability. The low energy footprints and synthesis and operating costs of our photo-responsive HCPs@Azo can potentially reduce carbon capture costs and establish a green carbon capture process driven by light.

Received 31st July 2023
Accepted 11th September 2023

DOI: 10.1039/d3ta04553f

rsc.li/materials-a

Introduction

The combustion of fossil fuels contributes to over 80% of the total energy produced in the world and releases 3×10^{13} kg of CO₂ every year,¹ accounting for 91% of anthropogenic CO₂ emissions.² Despite the transition into green energy, fossil fuel combustion is still expected to contribute to energy production for the next few decades.³ To realise the target of reducing 40% of CO₂ emissions in Europe by 2030 and achieving a net-zero greenhouse gas emission economy by 2050,⁴ it is imperative that carbon capture is energy-efficient and cost-effective.

Legacy carbon capture technologies are highly effective for reducing up to 90% of CO₂ emissions from power plants that produce energy *via* fossil fuel combustion.⁵ Carbon capture in power plants can be achieved through pre-, post-, and oxy fuel combustion approaches. In pre- and post-combustion, CO₂ is captured prior and after completion of the combustion process, respectively, while in oxy-fuel combustion capture, CO₂ flow is purified and condensed with other flue gases.⁶ Amine-based absorption, a chemical capture process,^{7,8} is the incumbent technology deployed for post-combustion carbon capture in power plants.⁹ However, amine absorption is costly and energy-intensive due to regeneration requirements and corrosive

nature of amines and can lead to environmental pollution when end-of-life amines are disposed.¹⁰

Physical processes like membrane technology^{11–14} and adsorption^{15,16} have also been explored for post-combustion capture. Compared to membrane separation, the advantages of adsorption by solid adsorbents include good stability, high reusability, flexibility, and comparatively lower costs than absorption.¹⁷ CO₂ adsorption in adsorbents is dependent on the electronic attraction between CO₂ molecules and adsorbent surfaces.¹⁸ Examples of such materials include activated carbons,¹⁹ zeolites,²⁰ metal-organic frameworks (MOFs)²¹ and hypercrosslinked polymers (HCPs).²² Likewise amine regeneration, regenerating these microporous adsorbents *via* traditional methods of temperature swing, pressure swing or vacuum swing is energy-intensive and costly.²³ For example, the operating costs of traditional carbon capture processes that rely on amine absorption or adsorption with zeolites cost around US\$50 per ton of CO₂.^{24,25} MOFs are regenerated at 120 °C–200 °C for at least 8 hours;²⁶ regeneration of activated carbon requires a vacuum to desorb CO₂ molecules;²⁷ regenerating HCPs require a temperature of 80 °C and vacuum pressure of 0.1 bar for 4 hours.²⁸ The energy consumption and cost of regenerating adsorbents can be potentially reduced with using renewable energy such as light to drive desorption (Fig. 1). The cost of carbon capture could be potentially reduced by >90% with light-induced swing adsorption processes as per the costs savings observed in light-controlled desalination.²⁹

Different light wavelengths can be exploited to change the inherent physical or chemical properties of microporous solid adsorbents to trigger CO₂ adsorption or desorption.³⁰ For

School of Engineering, The University of Edinburgh, Robert Stevenson Road, Edinburgh, EH9 3BF, UK. E-mail: cherhon.lau@ed.ac.uk

† Electronic supplementary information (ESI) available. See DOI: <https://doi.org/10.1039/d3ta04553f>

‡ These authors contributed equally to this work.

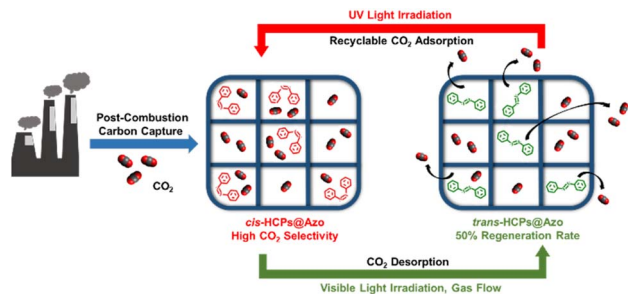


Fig. 1 Our approach of exploiting photo-isomerisation of azobenzene molecules embedded in pores of HCPs to drive adsorption (upon UV irradiation) and desorption (vis-irradiation) of CO₂ to enable low-energy, low-cost carbon capture.

example, the CO₂ adsorption capacities of photo-responsive MOFs of PCN-123 and T(7.5)/U-azo were reduced by 53.9% and 31.4%, respectively, upon UV-irradiation. This was attributed to blocking CO₂ access to adsorption sites (metal cluster and amine) by the *trans-cis* conformation change of pendant azobenzene groups.^{31,32} Conversely, the positive dipole moment (3.0 D) of *cis*-azobenzene triggered by UV irradiation could be exploited to increase the uptake capacity of CO₂ in porous organic polymer adsorbents.³³ Photo-irradiation of such adsorbents can also tailor and control desorption. For example, 42% of the CO₂ adsorbed in light-responsive MOFs Zn(AzDC)(4,4'-BPE)_{0.5} were desorbed through photo-reversible changes in MOF structures that were induced by *cis-trans* photo-isomerization of azobenzene-based ligands.²³ Vis-irradiation (400–500 nm visible light) of Ag/Uio-66 MOFs at 0.99 bar led to the desorption of 88.2% of CO₂ as Ag converted light energy to thermal energy that aided desorption.³⁴ Meanwhile, photo-irradiation of porous aromatic frameworks comprising diarylethene photo-switches, with 200–500 nm unfiltered light, weakened CO₂-adsorbent interactions,³⁵ desorbing up to 26% of adsorbed CO₂ within 4 minutes.³⁶ Although these works demonstrate the potential of photo-modulated carbon capture and adsorbent regeneration, the cost and operation of photo-sensitive adsorbents for such applications have not been evaluated in comparison with traditional regeneration methods (thermal and vacuum) and studied with gas mixtures representative of post-combustion flue gas compositions.

Herein we deployed photo-responsive HCPs loaded with 8.9 wt% azobenzene (HCPs@Azo) that were developed in our previous work³⁷ in simulated post-combustion flue gas mixtures (CO₂ 4–20 v/v% in N₂) to address this knowledge gap. Upon UV-irradiation, the azobenzene molecules incorporated within HCP pores undergo a photo-reversible *trans-cis* isomerization caused by $n\text{-}\pi^*$ and $\pi\text{-}\pi^*$ excitations,³⁸ leading to changes in physical dimensions and dipole moment, from 9 Å (*trans*) to 5.5 Å (*cis*),³⁹ and 0 D (*trans*) to 3.0 D (*cis*),⁴⁰ respectively. Here we observed that these UV-triggered photo-reversible changes enhanced the CO₂ adsorption capacity of HCPs@Azo by 48%, from 1 mmol g^{−1} to 1.48 mmol g^{−1}. This was 17% higher than that of pristine HCPs (1.26 mmol g^{−1}). In a gas mixture comprising 20 v/v% CO₂, CO₂ adsorption capacity and CO₂/N₂ selectivity of *cis*-

HCPs@Azo were concomitantly improved by 12% and 76%, respectively, compared to those of HCPs, reaching 0.67 mmol g^{−1} and 31.6 mmol g^{−1}. 14% of the CO₂ adsorbed on these adsorbents were desorbed upon vis-irradiation, demonstrating the feasibility of light-controlled carbon capture and regeneration in simulated flue gas conditions. In addition, the photo-modulated adsorption and desorption capacities stabilised after 5 cycles of application. The use of light to recover the adsorption capacities of HCPs@Azo was only 50% as effective as traditional temperature and vacuum swing methods, but the total cost of our approach was only one-five-hundredth of the cost of these legacy methods.

Experimental section

Materials

All solvents, reagents and chemicals were purchased from Alfa Aesar, Sigma-Aldrich and Fisher Chemical without any purification before using. Iron chloride (FeCl₃) and 1,2-dichloroethane (DCE) were obtained from Alfa Aesar. Azobenzene and formaldehyde dimethyl acetal (FDA) were purchased from Sigma-Aldrich. Methanol, ethanol, chloroform and acetone were received from Fisher Chemical. Waste expanded polystyrene (tradename: Styrofoam) was collected from discarded packaging supplies around The University of Edinburgh and used as is.

Synthesis of photo-sensitive HCPs

HCPs were first synthesized using the protocol developed in our group,⁴¹ where the reactants mass ratio were maintained at 1 : 5 : 5. 1 g Styrofoam was added into a 100 mL flask and dissolved by 50 mL of DCE. 5 g FeCl₃ (catalyst) and 5 g FDA (external crosslinker) were added into above mixture, and the new mixture was stirred and refluxed for 24 hours with 80 °C and 270 rpm stirring. The HCPs were synthesised *via* Friedel–Crafts alkylation reactions. The product was collected by vacuum suction filtration, and washed by chloroform, methanol, acetone, and deionized water for 3 times respectively. The washed solid was dried in a vacuum oven at 120 °C for 12 hours to obtain brown HCPs powder.

HCPs@Azo were fabricated using our previously reported protocol.³⁷ Briefly, 500 mg azobenzene was dissolved in 20 mL of ethanol. 200 mg of HCPs were steeped into the azobenzene ethanolic solution for 12 hours to reach equilibrium. To remove azobenzene molecules that were adsorbed on the surface of HCPs, the brown product was washed with ethanol for 10 seconds and dried at room temperature for 12 hours to yield HCPs@Azo.

Experimental configuration for adsorption and desorption

Dynamic adsorption and photo-modulated desorption measurements for HCPs and HCPs@Azo were taken at room temperature (25 °C) and atmospheric pressure. These measurements were taken using a laboratory-scale self-made fixed-bed apparatus (Fig. 2). A self-programmed Labview data collection software was utilised to record the monitored





Fig. 2 Experimental configuration for adsorption: (1) N₂ gas cylinder and regulator, (2) CO₂ gas cylinder and regulator, (3) zeolite/silica drying column of N₂ gas, (4) zeolite/silica drying column of CO₂ gas, (5) mass flow controller of N₂ (Brooks Instruments GF-Series, range: 0–400 mL min^{−1}), (6) mass flow controller of CO₂ (Brooks Instruments GF-Series, range: 0–100 mL min^{−1}), (7) fibre-optic temperature sensor and signal conditioner, (8) data analysis workstation, (9) metal retainer, (10) quartz container (12 mm inner diameter, 1 mm wall thickness), (11) water condenser, (12) non-dispersive infrared CO₂ sensor (COZIR-W-100, calibration range: 0–70% v/v), (13) mass flow meter (Brooks Instruments SLA5860, range: 0–500 mL min^{−1}), and (14) gas exit.

variables (temperature, flow rate, humidity, and CO₂ concentration) every second from the beginning of the adsorption experiment. Desorption of CO₂ from adsorbents were performed immediately after adsorption using visible light irradiation (brand: ZLUV LAMP, power: 6 W) in the same quartz container (Fig. S1†).

Photo-modulated gas adsorption experiments

Dry gas mixtures comprising 0 to 100 v/v% of CO₂ in N₂ were allowed to flow in an empty quartz container under test gas flow rates. The humidity sensor indicated undetectable moisture levels. Data from these experiments was plotted as a concentration curve for subsequent determination of adsorbed CO₂ quantities.

500 mg HCPs and 1 g HCPs@Azo were used here for gas adsorption experiments. First, 500 mg of HCPs@Azo were irradiated with 450 nm visible light for 1 hour to ensure that all azobenzene molecules in HCPs@Azo were in the *trans* state. The other 500 mg of HCPs@Azo were irradiated with 365 nm UV light (brand: ZLUV LAMP, power: 6 W, light intensity: 610 mW cm^{−2}) to yield *cis*-HCPs@Azo. HCPs, *trans*-HCPs@Azo and *cis*-HCPs@Azo were loaded into the quartz container respectively, and the container was fixed in the metal retainer. Gas was introduced at the top of the container through a small quartz container. All gas lines were swept with N₂ before and between experiments. The gas flow rates for pure CO₂ and pure N₂ adsorption test were maintained at 10 mL min^{−1}, regulated with two calibrated mass flow controllers.

For mixed gas adsorption experiments, CO₂ concentration in the inflow gas was varied by adjusting the input ratio of N₂ and CO₂ at fixed flow rates of 20 mL min^{−1}. For a mixed gas comprising 1 v/v% CO₂, the total rate flow of gases was 100

mL min^{−1}. The adsorption rate (r_{ads} , mmol g^{−1} s^{−1}) and capacity (q_{ads} , mmol g^{−1}) were calculated according to the following equations:

$$r_{\text{ads}} = \frac{1}{m} \times \frac{P_{\text{ads}}}{R \times T_{\text{ads}}} \times \left(V_{\text{blank,CO}_2} - \frac{C_{\text{out,CO}_2}}{C_{\text{blank,CO}_2}} \times V_{\text{blank,CO}_2} \right) \quad (1)$$

$$q_{\text{ads}} = \int_0^t r_{\text{ads}} dt \quad (2)$$

where $C_{\text{blank,CO}_2}$ (mg L^{−1} s^{−1}) and $V_{\text{blank,CO}_2}$ (mL s^{−1}) are the concentration and volume of CO₂ of blank experiment, $C_{\text{out,CO}_2}$ (mg L^{−1} s^{−1}) is the concentration of CO₂ at outlet of the experiment system, T_{ads} (K) and P_{ads} (kPa) are the temperature and pressure of adsorption process, R is the gas constant (8.314 J mol^{−1} K^{−1}), m (g) is the mass of adsorbents, t (s) is the duration of adsorption.

Desorption experiments

HCPs, *trans*-HCPs@Azo and *cis*-HCPs@Azo that were used to adsorb CO₂ from pure CO₂ gas in adsorption experiments were collected, weighed, and used in desorption experiments. At the start of desorption experiments, pure N₂ gas (flow rate of 20 mL min^{−1}) was used to purge possible residual CO₂ in the gas line, and as sweep gas throughout this experiment. Here we performed these experiments with two sets of conditions – one without visible light irradiation where CO₂-loaded adsorbents were loaded directly into the quartz container and the sweep gas of N₂ was used to facilitate desorption, while in another set of experiments, visible light irradiation (450 nm wavelength) was used to trigger desorption. In the latter set of experiments, after loading adsorbents into the quartz container, N₂ sweep gas was introduced alongside vis-irradiation simultaneously. The desorption rate (r_{des} , mmol g^{−1} s^{−1}) and desorption capacity (q_{des} , mmol g^{−1}) were calculated using these equations:

$$r_{\text{des}} = \frac{1}{m} \times \frac{1}{M_{\text{CO}_2}} \times \left(\frac{C_{\text{out,CO}_2} \times M_{\text{CO}_2}}{M_{\text{Air}}} \times V_{\text{mf}} - \frac{C_{\text{blank,CO}_2} \times M_{\text{CO}_2}}{M_{\text{Air}}} \times V_{\text{blank}} \right) \quad (3)$$

$$q_{\text{des}} = \int_0^t r_{\text{des}} dt \quad (4)$$

where $C_{\text{blank,CO}_2}$ and $C_{\text{out,CO}_2}$ (mg L^{−1} s^{−1}) are the concentrations of CO₂ of blank experiment and the outlet after desorption, V_{blank} (mL s^{−1}) and V_{mf} (mL s^{−1}) are the volumes of total volume of gas before and after desorption process, M_{CO_2} and M_{Air} are the relative molecular mass of CO₂ and air, m (g) is the mass of spent adsorbents, t (s) is the duration of desorption.

Photo-modulated cyclic adsorption and desorption

These experiments were performed using a simulated flue gas mixture with 20 v/v% CO₂. 500 mg of HCPs@Azo was first UV-irradiated for 1 hour and the resultant *cis*-HCPs@Azo samples were used to adsorb CO₂. After adsorption, the CO₂-loaded *cis*-HCPs@Azo adsorbents were vis-irradiated for 1 hour, under continuous N₂ flow. Subsequently, the regenerated *trans*-



HCPs@Azo adsorbents were irradiated with UV light again for the next adsorption cycle. The above adsorption-regeneration cycling was repeated 5 times to study the reusability of HCPs@Azo. The regeneration efficiency (R) of HCPs@Azo was evaluated by the following equation:

$$R = \frac{q_{\text{ads}}}{q_{\text{ads(L)}}} \quad (5)$$

where q_{ads} (mmol g^{-1}) and $q_{\text{ads(L)}}$ (mmol g^{-1}) are the adsorption capacities of HCPs@Azo prior and after desorption, respectively.

Results and discussion

CO₂ adsorption capacity and CO₂/N₂ selectivity

We previously showed that the photo-responses of azobenzene molecules embedded within HCP pores could be exploited to enhance and reduce CO₂ uptake as a function of photo-irradiation wavelength.³¹ The CO₂ uptake (determined using pure CO₂ at 273 K and 1 bar) of HCPs, *cis*-HCPs@Azo and *trans*-HCPs@Azo reached 2.08 mmol g⁻¹, 2.54 mmol g⁻¹ and 1.48 mmol g⁻¹, respectively. This could be ascribed to an increment in BET specific surface areas and a positive dipole moment that are associated with the *trans*-*cis* isomerization of azobenzene from 9 Å to 5.5 Å. The BET surface area of *cis*-HCPs@Azo reached 1024 m² g⁻¹, 19% higher than the BET specific surface area of *trans*-HCPs@Azo (862 m² g⁻¹). In addition, computational simulations showed that the 22% increase in CO₂ uptake of *cis*-HCPs@Azo from pristine HCPs was due to dipole-quadrupole interactions between UV irradiated *cis* state azobenzene molecules (3.0 D) and CO₂ molecules ($-13.4 \pm 0.4 \times 10^{-40} \text{ cm}^2$).⁴² These mechanisms were also responsible for the trends observed here when CO₂ adsorption capacities were determined using a breakthrough rig at room temperature (298 K) and atmospheric pressure with a pure CO₂ flow rate of 10 mL min⁻¹ over 600 seconds (Fig. 3). The CO₂ adsorption

capacity of *cis*-HCPs@Azo reached 1.48 mmol g⁻¹, 48% and 17% higher than those of *trans*-HCPs@Azo (1 mmol g⁻¹) and HCPs (1.26 mmol g⁻¹), respectively.

The N₂ adsorption capacities of HCPs, *cis*-HCPs@Azo and *trans*-HCPs@Azo were also determined using pure N₂ gas with a flow rate of 10 mL min⁻¹ at room temperature and atmospheric pressure (Table S2†). We used this data to calculate the ideal CO₂/N₂ selectivity using Equation in Table S2†^{43,44} (Fig. 3). Similar to other microporous adsorbents,^{45,46} the CO₂ adsorption capacities of all HCP types studied here in this work were higher than those of N₂. The CO₂/N₂ selectivity of both pristine HCPs and *trans*-HCPs@Azo were similar, reaching a value of 9 while the CO₂/N₂ selectivity of *cis*-HCPs@Azo was 47% higher, reaching a value of 13.3. In addition to a 3.0 D dipole moment that enhanced dipole-quadrupole interactions with CO₂ molecules,⁴¹ *cis* state azobenzene molecules in *cis*-HCPs@Azo could contribute to additional van der Waals forces⁴⁷ that consequently attracted more CO₂ than N₂ molecules. With higher CO₂ adsorption capacity and CO₂/N₂ selectivity, *cis*-HCPs@Azo studied here were better adsorbents for carbon capture than pristine HCPs.

The mixed gas adsorption capacities and CO₂/N₂ selectivities of all HCP types studied here in this work were determined using CO₂/N₂ gas mixtures comprising 1 v/v% of CO₂ (for minimising the risk of headaches⁴⁸), 10 v/v% and 20 v/v% of CO₂ to simulate post-combustion flue gas streams,⁴⁹ and 40 v/v% of CO₂ to simulate high CO₂ content environments (Fig. S3†). As shown in Fig. 4a, the adsorption capacities of all three adsorbents studied here increased rapidly when CO₂ content was between 1–40 v/v%. At 1 v/v% CO₂, the CO₂ adsorption capacities of pristine HCPs, *cis*-HCPs@Azo and *trans*-HCPs@Azo were identical. As CO₂ concentration increased, the adsorption capacities of *cis*-HCPs@Azo were higher those that of pristine HCPs and *trans*-HCPs@Azo. For example, at 20 v/v% CO₂, the adsorption capacity of *cis*-HCPs@Azo (0.67 mmol g⁻¹) was 12% and 46% higher those that of pristine HCPs (0.6 mmol g⁻¹) and *trans*-HCPs@Azo (0.46 mmol g⁻¹), respectively. Beyond 40 v/v% CO₂, the increment rates in CO₂ adsorption capacities were less pronounced, possibly due to saturated adsorption sites. The mixed gas adsorption capacities of these adsorbents were lower than those obtained from pure gases. This could be attributed



Fig. 3 CO₂ adsorption profiles of (black) HCPs, (green) visible light irradiated *trans*-HCPs@Azo and (red) UV light irradiated *cis*-HCPs@Azo using a flow rate of 10 mL min⁻¹, pure CO₂ gas, at room temperature and atmosphere pressure. CO₂/N₂ ideal selectivities of HCPs, *trans*-HCPs@Azo and *cis*-HCPs@Azo were obtained using CO₂ and N₂ pure gas adsorption capacities after 600 s (Table S2†).^{43,44}

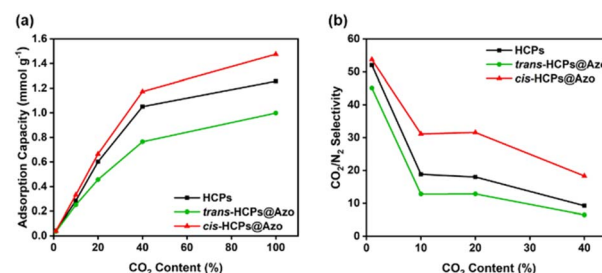


Fig. 4 (a) CO₂ adsorption capacities and (b) mixed gas CO₂/N₂ selectivities (Table S3†)^{51,52} of (black) HCPs, (green) *trans*-HCPs@Azo and (red) *cis*-HCPs@Azo at different CO₂ concentration of 1 v/v%, 10 v/v%, 20 v/v%, 40 v/v% and 100 v/v% at room temperature (25 °C) and atmosphere pressure (1 bar).



to lower CO₂ content in gas mixtures and competitive sorption.⁵⁰

Competitive sorption between CO₂ and N₂ gas molecules was also why the mixed gas selectivities of HCPs, *cis*-HCPs@Azo and *trans*-HCPs@Azo at 1–20 v/v% CO₂ (determined from mole fraction of CO₂ and N₂ in gas feed and output (Table S3†)^{51,52}) were 476–99%, 305–138% and 400–43% higher than their ideal CO₂/N₂ selectivities (Fig. 4b). As CO₂ concentration increased to 40 v/v%, the mixed gas CO₂/N₂ selectivity of only *cis*-HCPs@Azo was higher than its ideal selectivity. This was most probably due to the synergistic effects of both dipole–quadrupole interactions and competitive sorption. At 10 v/v% and 20 v/v% CO₂, *i.e.*, simulated flue gas concentrations, the mixed gas CO₂/N₂ selectivity of pristine HCPs studied in this work were similar to the CO₂/N₂ selectivity of similar HCPs that were determined using the ideal adsorbed selectivity theory (IAST).⁴¹ We also observed that the mixed gas CO₂/N₂ selectivity of HCPs, *cis*-HCPs@Azo and *trans*-HCPs@Azo decreased as CO₂ concentration in the feed gas increased from 1 to 40 v/v%. This was because more CO₂ molecules were left in the feed as saturated CO₂ adsorption sites limited further uptake.⁵³ Amongst all adsorbents studied here, *cis*-HCPs@Azo are potentially suited for post-combustion carbon capture. This was because, at 20 v/v% CO₂, the CO₂/N₂ selectivity of *cis*-HCPs@Azo reached 31.6, which was 145% and 76% higher than that of *trans*-HCPs@Azo (12.9) and pristine HCPs (18).

Kinetics of photo-modulated gas adsorption

Three kinetic models – pseudo-first order, pseudo-second order and Avrami's fractional order (Fig. S4†) were deployed here to reveal the gas-adsorbent interactions and adsorption rate behaviour⁵⁴ of all adsorbents studied in this work. The pseudo-first order model⁵⁵ assumes that the adsorption rate is proportional to the number of free adsorption sites⁵⁶ and is typically used to explain the physical adsorption process⁵⁷ *via* the following equation:

$$q_t = q_e(1 - e^{-k_1 t}) \quad (6)$$

where q_t (mmol g⁻¹) and q_e (mmol g⁻¹) are the amounts of adsorbed CO₂ per unit of adsorbents at any time, t (s) and at equilibrium, k_1 (s⁻¹) is the rate constant of Pseudo-first order model. The pseudo-second order model⁵⁸ assumes that the adsorption process is most likely controlled by chemical adsorption⁵⁹ and can be expressed as:

$$q_t = \frac{q_e^2 k_2 t}{1 + q_e k_2 t} \quad (7)$$

where k_2 (g mmol⁻¹ s⁻¹) is the rate constant of Pseudo-second order process. Avrami's fractional order model describes the process of random nucleation and subsequent growth.⁶⁰ This kinetic model assumes the adsorption process is a complex process including physical and chemical adsorption⁶¹ and can be described with the following equation:

$$q_t = q_e(1 - e^{-(k_A t)^{n_A}}) \quad (8)$$

where k_A (s⁻¹) is the Avrami kinetic model constant, n_A is the kinetic order of the Avrami model. n_A is the Avrami exponent which is a fractionary number to reflect the possible change of mechanism during adsorption.⁶² The term n_A expresses the dimensionality of growth of adsorption sites, where $n_A = 2$ represents one-dimensional growth, $n_A = 3$ is for two-dimensional growth, $n_A = 4$ is for three-dimensional growth.⁵⁴ It is important to note that with a homogenous adsorption process, the probability of adsorption is identical at any region for any fixed time interval, $n_A = 1$.⁵⁴

Here, the CO₂ experimental adsorption data of HCPs, *cis*-HCPs@Azo and *trans*-HCPs@Azo fit better with Avrami's fractional order model where the correlation coefficient (R^2) was the highest (Table 1). This indicated that CO₂ adsorption process in these adsorbents demonstrated both physical and chemical behaviours.⁶³ With Avrami exponent (n_A) values between 0.9–1, adsorption in all three adsorbents studied here could be described as a homogenous and physical adsorption process. We also observed that the experimental CO₂ adsorption data could fit better with the pseudo-first order model than the pseudo-second order model, particularly for *cis*-HCPs@Azo. This meant that physical adsorption was more prevalent than chemical adsorption in *cis*-HCPs@Azo than pristine HCPs and *trans*-HCPs@Azo. This was most likely due to the additional van der Waals forces associated with dipole–quadrupole interactions between CO₂ and *cis*-state azobenzene molecules. Although the rate constants k_1 and k_A of *cis*-HCPs@Azo were larger than those of *trans*-HCPs@Azo, they remained smaller than that of pristine HCPs. This indicated that the CO₂ affinity of *cis* state azobenzene molecules could enhance adsorption rates, but could not offset adsorption rate losses associated with the loss in accessible pore volume due to the presence of azobenzene molecules in HCP pores.

Photo-modulated CO₂ desorption

Like other HCPs,^{37,64,65} CO₂ desorption from pristine HCPs in this work could only be enabled by thermal methods where a high temperature of 110 °C and a vacuum environment was

Table 1 Parameters of pseudo-first order, pseudo-second order and Avrami's fractional order kinetic models for pure CO₂ adsorption of HCPs, *trans*-HCPs@Azo and *cis*-HCPs@Azo with 10 mL min⁻¹ gas flow rate at room temperature and atmosphere pressure

Kinetic models	Pseudo-first order					Pseudo-second order					Avrami's fractional order					
	$q_{e,\text{exp}}$	mmol g ⁻¹	$q_{e,\text{cal}}$	mmol g ⁻¹	k_1 s ⁻¹	R^2	$q_{e,\text{cal}}$	mmol g ⁻¹	k_2 g mmol ⁻¹ s ⁻¹	R^2	$q_{e,\text{cal}}$	mmol g ⁻¹	k_A s ⁻¹	n	R^2	
HCPs	1.257		1.29		0.00565	0.9987	1.691		0.00309		0.9982	1.317		0.00542	0.9474	0.9991
<i>trans</i> -HCPs@Azo	0.998		1.09		0.00444	0.9993	1.5		0.00246		0.9979	1.102		0.00433	0.9765	0.9994
<i>cis</i> -HCPs@Azo	1.476		1.567		0.00491	0.9998	2.121		0.002		0.9979	1.57		0.00489	0.9956	0.9998



required. Meanwhile, visible light (450 nm) was used here to trigger CO₂ desorption from *trans*-HCPs@Azo and *cis*-HCPs@Azo. Here we used a N₂ sweep gas and visible light to desorb CO₂ molecules from adsorbents that were first exposed to pure CO₂ gas (Fig. 5). Without vis-irradiation, the CO₂ desorption capacities, and efficiencies of all three adsorbents only reached 0.046 mmol g⁻¹ and <5%. This showed that even with a sweep gas flow rate of 20 mL min⁻¹, CO₂ molecules could not be desorbed from adsorbents studied here. With 1.48 mmol g⁻¹ of CO₂ adsorbed in *cis*-HCPs@Azo, vis-irradiation of these adsorbents for 1 hour desorbed 0.21 mmol g⁻¹ of CO₂, reaching a CO₂ desorption efficiency of 14.2% (Fig. S5†). Compared to CO₂ desorption that were enabled by a N₂ sweep gas, vis-irradiation enhanced CO₂ desorption by 358%. CO₂ desorption from our photo-responsive HCPs was only enabled with vis-irradiation as the 3.0 D dipole moment of *cis*-azobenzene was reduced to 0 D (*trans*-azobenzene). Without dipole–quadrupole interactions between CO₂ and azobenzene molecules, a 20 mL min⁻¹ N₂ sweep gas could then easily remove these CO₂ molecules from the adsorbent surface. Additionally, *cis*–*trans* isomerisation of azobenzene also reduced the accessible pore volume,³⁷ where the physical dimensions of azobenzene increased from 5.5 Å to 9 Å could force out CO₂ molecules from the pores. Here, it is important to highlight that although vis-modulated desorption efficiency could only reach 14%, this could be potentially improved by ensuring that all *cis*-HCPs@Azo that were packed into the quartz container were exposed to the light source. Currently, only *cis*-HCPs@Azo on the outermost surface of the quartz container were exposed to visible light. Moreover, there were only 8.9 wt% of azobenzene molecules present in HCP pores and CO₂ adsorption could still take place in pores that were not loaded with azobenzene. Hence, even with photo-irradiation, CO₂ molecules present in

pores without azobenzene could remain adsorbed. Therefore, another approach to potentially enhance desorption efficiency and capacity is to ensure that all pores are loaded with azobenzene molecules. Through a series of complementary control experiments (gas adsorption and desorption without photo-irradiation in the presence of a sweep gas), we isolated the effects of photo-irradiating 8.9 wt% azobenzene in HCPs on CO₂ adsorption and desorption, where UV-irradiation led to the adsorption 0.48 mmol g⁻¹ more CO₂ and vis-irradiation desorbed 0.2 mmol g⁻¹ of CO₂. This meant that the desorption efficiency attributed to the presence of azobenzene in HCPs reached 42%.

Kinetics of photo-modulated gas desorption

To further understand the desorption process, the desorption experimental data of three adsorbents, with/without visible light irradiation under pure N₂ gas flow at room temperature and atmospheric pressure, were fitted with the following kinetic models:

Pseudo-first order model:

$$q_{Dt} = q_{De}(1 - e^{-k_1 t}) \quad (9)$$

Pseudo-second order model:

$$q_{Dt} = \frac{q_{De}^2 k_2 t}{1 + q_{De} k_2 t} \quad (10)$$

Avrami's fractional order model:

$$y = 1 - e^{-(k_A t)^{n_A}} \quad (11)$$

where q_{Dt} (mmol g⁻¹) and q_{De} (mmol g⁻¹) are the amount of desorbed CO₂ per unit mass of adsorbents at any time, t (s) and



Fig. 5 The rate and capacities of adsorption (blue solid line) and desorption process (no visible irradiation: black dashed line; visible irradiation: red dotted line) of (a) HCPs, (b) *cis*-HCPs@Azo and *trans*-HCPs@Azo.



Table 2 Parameters of pseudo-first order, pseudo-second order and Avrami's fractional order kinetic models for CO₂ desorption from HCPs, HCPs-vis, *cis*-HCPs@Azo, *cis*-HCPs@Azo-vis and *trans*-HCPs@Azo at room temperature and atmosphere pressure

Kinetic models	Pseudo-first order				Pseudo-second order			Avrami's fractional order			
	$q_{e,exp}$ mmol g ⁻¹	$q_{e,cal}$ mmol g ⁻¹	k_1 s ⁻¹	R^2	$q_{e,cal}$ mmol g ⁻¹	k_2 g mmol ⁻¹ s ⁻¹	R^2	$q_{e,cal}$ mmol g ⁻¹	k_A s ⁻¹	n	R^2
HCPs	0.0457	0.122	4.3×10^{-4}	0.9823	0.23	0.001	0.9818	0.0485	0.00161	1.673	0.9999
HCPs-vis	0.0464	0.122	4.5×10^{-4}	0.9789	0.16	0.0022	0.9763	0.0483	0.00166	1.747	0.9996
<i>cis</i> -HCPs@Azo	0.0463	0.131	4.2×10^{-4}	0.9669	0.18	0.0017	0.965	0.0472	0.00174	1.986	0.9998
<i>cis</i> -HCPs@Azo-vis	0.2057	0.219	0.0031	0.9501	0.29	0.0092	0.928	0.1585	0.01	0.913	0.5541
<i>trans</i> -HCPs@Azo	0.0401	0.055	0.0013	0.9869	0.086	0.0096	0.9835	0.0415	0.00202	1.456	0.9999

at equilibrium, k_1 (s⁻¹), k_2 (g mmol⁻¹ s⁻¹) and k_A (s⁻¹) are the rate constant of pseudo-first order, Pseudo-second order and Avrami's fractional order model respectively, y is desorption fraction, $y = q_{Dt}/q_{De}$, n_A is the Avrami exponent.

Regardless of vis-irradiation, in the presence of a N₂ sweep gas, CO₂ desorption in pristine HCPs and *trans*-HCPs@Azo could be described using the Avrami fractional order model (Table 2, Fig. S5†) because of the higher correlation coefficient R^2 obtained when compared to those fitted using pseudo-first order and pseudo-second order models. This meant that the desorption mechanisms in these adsorbents were not based on either pure physical or chemical desorption. Meanwhile n_A of these four desorption processes were between 1 and 2, indicative that these desorption processes occurred *via* a variety of pathways.⁵² Experimental desorption data from these four processes fit better with the pseudo-first order model than the pseudo-second order, indicating that physical adsorption was more prevalent in these four desorption processes. The CO₂ desorption data of *cis*-HCPs@Azo that was obtained by vis-irradiation fit better with the pseudo-first order model, where the highest R^2 value reached 0.9501 amongst all kinetic models used here. This inferred that vis-triggered desorption of CO₂ from *cis*-HCPs@Azo demonstrated characteristics of both physical and chemical processes, with the former being more prevalent. More CO₂ molecules were desorbed from *cis*-HCPs@Azo upon vis-irradiation as the *cis-trans* isomerization of azobenzene reverted led to a loss of physical van der Waals forces and dipole-quadrupole interactions for CO₂ attraction towards the adsorbent surface.

Reusability of photo-sensitive HCPs

Here we used our protocols for photo-modulated adsorption and desorption to evaluate the reusability of HCPs@Azo over five cycles using a gas mixture that simulated post-combustion flue gas streams that contained 20 v/v% CO₂ (Fig. 6). After three cycles of photo-triggered adsorption and desorption, the loss in adsorption capacities of HCPs@Azo stabilised. The main reason for this loss was that pores without azobenzene in HCPs@Azo were unable to undergo reversible photo-induced changes in textural properties (BET surface area, accessible pore volume and sizes) and dipole moment. Hence, the CO₂ adsorbed in these pores, like in pristine HCPs, could not be desorbed by visible light irradiation, and remained in the pores.

Consequently, this hindered subsequent adsorption. By the fourth and fifth cycles, the regeneration efficiency of HCPs@Azo reached 100% and 95% (Fig. 6), delivering experimental working capacities of 0.38–0.36 mmol g⁻¹ that were identical to those of legacy CO₂ adsorbent materials deployed in temperature swing adsorption.⁶⁶ The stable regeneration efficiency also indicated that the azobenzene guest molecules did not leach from HCPs@Azo. In a separate study from our group [DOI: 10.2139/ssrn.4535503], we also showed that azobenzene molecules did not leach out from HCPs@Azo even after immersion in water for up to 4.5 hours. Hence HCPs@Azo will remain relatively stable even when gas mixtures containing moisture are used (similar to real-world conditions). Here it is important to highlight that azobenzene molecules could leach out from HCPs@Azo when they come into contact with vapors of organic solvents such as alcohol,⁶⁷ ether⁶⁸ and glacial acetic acid.⁶⁹ However, such vapors are not present in feed streams of most carbon capture processes.⁷⁰ In addition, we also compared the energy consumption and cost for one adsorption-desorption cycle enabled with a high temperature of 110 °C and vacuum, and our photo-modulated approach (Table S4†). Using an average electricity price of £0.34 per kWh in 2023 in UK,⁷¹ the cost of thermal regeneration reached £2.04 while our photo-modulated approach cost only £0.004. Clearly, our approach of photo-modulated regeneration is more cost-effective and less energy-intensive than traditional regeneration methods.



Fig. 6 (Column) adsorption capacity and (red line) regeneration efficiency of HCPs@Azo in five adsorption-desorption cycles using UV and visible light irradiation.



Conclusions

Using HCPs@Azo developed in our previous work, here we experimentally demonstrate the feasibility and benefits of deploying photo-responsive adsorbents for post-combustion carbon capture. Through a series of control experiments, we were able to isolate the effects of photo-modulation on regenerating HCPs@Azo. With 8.9 wt% azobenzene in HCPs, 0.48 mmol g⁻¹ more CO₂ was adsorbed in *cis*-HCPs@Azo from a CO₂-N₂ mixture comprising only 20 v/v% CO₂. Vis-irradiation of this CO₂-loaded adsorbent, led to the desorption of 0.2 mmol g⁻¹ CO₂. As such, the working capacity of HCPs@Azo based on the amount of azobenzene present, reached 41.6%, comparable to those of legacy CO₂ adsorbents deployed in temperature swing adsorption and other state-of-art photo-responsive adsorbents. Calculations show that the energy footprint and costs of our photo-modulated regeneration approach was a fraction of those of legacy regeneration approaches. We also identified possible methods to improve regeneration efficiency, for *e.g.*, increasing azobenzene content in HCPs whilst ensuring that all HCP pores contain these photo-switches. Outcomes from this work could potentially establish photo-modulated regeneration as a low-cost, low-carbon approach for post-combustion carbon capture.

Author contributions

AL and GL contributed equally to performing experiments and data analyses. The research concept was developed by AL and CHL. XF provided guidance and the setup for mixed gas adsorption experiments. All authors contributed to editing and writing this paper.

Conflicts of interest

There are no conflicts to declare.

References

- 1 X. Fan, *Handbook of Clean Energy Systems*, 2015, pp. 1–30.
- 2 S. J. McGurk, C. F. Martín, S. Brandani, M. B. Sweatman and X. Fan, *Appl. Energy*, 2017, **192**, 126–133.
- 3 N. Ghorbani, A. Aghahosseini and C. Breyer, *Renewable Energy*, 2020, **146**, 125–148.
- 4 C. Chao, Y. Deng, R. Dewil, J. Baeyens and X. Fan, *Renewable Sustainable Energy Rev.*, 2021, **138**, 110490.
- 5 T. C. Drage, C. E. Snape, L. A. Stevens, J. Wood, J. Wang, A. I. Cooper, R. Dawson, X. Guo, C. Satterley and R. Irons, *J. Mater. Chem.*, 2012, **22**, 2815–2823.
- 6 M. Kanniche, R. Gros-Bonnivard, P. Jaud, J. Valle-Marcos, J.-M. Amann and C. Bouallou, *Appl. Therm. Eng.*, 2010, **30**, 53–62.
- 7 R. Quinn, R. J. Kitzhoffer, J. R. Hufton and T. C. Golden, *Ind. Eng. Chem. Res.*, 2012, **51**, 9320–9327.
- 8 H. Jilvero, *Ammonia as an Absorbent of Carbon Dioxide in Post-Combustion Capture-An Experimental, Technical and Economic Process Evaluation*, Chalmers Tekniska Hogskola, Sweden, 2014.
- 9 V. Gargiulo, M. Alfè, F. Raganati, L. Lisi, R. Chirone and P. Ammendola, *Fuel*, 2018, **222**, 319–326.
- 10 F. Raganati, F. Miccio and P. Ammendola, *Energy Fuels*, 2021, **35**, 12845–12868.
- 11 E. Lasseguette, M.-C. Ferrari and S. Brandani, *Energy Procedia*, 2014, **63**, 194–201.
- 12 M. Sandru, T.-J. Kim, W. Capala, M. Huijbers and M.-B. Hägg, *Energy Procedia*, 2013, **37**, 6473–6480.
- 13 S. He, B. Zhu, S. Li, Y. Zhang, X. Jiang, C. H. Lau and L. Shao, *Sep. Purif. Technol.*, 2022, **284**, 120277.
- 14 B. Zhu, S. He, Y. Wu, S. Li and L. Shao, *Engineering*, 2022, DOI: [10.1016/j.eng.2022.03.016](https://doi.org/10.1016/j.eng.2022.03.016).
- 15 J. Merel, M. Clausse and F. Meunier, *Ind. Eng. Chem. Res.*, 2008, **47**, 209–215.
- 16 T.-H. Bae, M. R. Hudson, J. A. Mason, W. L. Queen, J. J. Dutton, K. Sumida, K. J. Micklash, S. S. Kaye, C. M. Brown and J. R. Long, *Energy Environ. Sci.*, 2013, **6**, 128–138.
- 17 A. A. Abd, S. Z. Naji, A. S. Hashim and M. R. Othman, *J. Environ. Chem. Eng.*, 2020, **8**, 104142.
- 18 D. M. Ruthven, *Principles of Adsorption and Adsorption Processes*, John Wiley & Sons, 1984.
- 19 H. M. Coromina, D. A. Walsh and R. Mokaya, *J. Mater. Chem. A*, 2016, **4**, 280–289.
- 20 S. Chen, M. Zhu, Y. Fu, Y. Huang, Z. Tao and W. Li, *Appl. Energy*, 2017, **191**, 87–98.
- 21 J. A. Mason, K. Sumida, Z. R. Herm, R. Krishna and J. R. Long, *Energy Environ. Sci.*, 2011, **4**, 3030–3040.
- 22 S. Yao, X. Yang, M. Yu, Y. Zhang and J.-X. Jiang, *J. Mater. Chem. A*, 2014, **2**, 8054–8059.
- 23 R. Lyndon, K. Konstantas, B. P. Ladewig, P. D. Southon, P. C. J. Keperter and M. R. Hill, *Angew. Chem.*, 2013, **125**, 3783–3786.
- 24 M. T. Ho, G. W. Allinson and D. E. Wiley, *Ind. Eng. Chem. Res.*, 2008, **47**, 4883–4890.
- 25 F. Su and C. Lu, *Energy Environ. Sci.*, 2012, **5**, 9021–9027.
- 26 P. Küsgens, A. Zgaverdea, H. G. Fritz, S. Siegle and S. Kaskel, *J. Am. Ceram. Soc.*, 2010, **93**, 2476–2479.
- 27 Q. Cen, M. Fang, T. Wang, I. Majchrzak-Kucęba, D. Wawrzyńczak and Z. Luo, *Greenhouse Gases: Sci. Technol.*, 2016, **6**, 787–796.
- 28 F. Maleki, A. Ghaemi and G. Mir Mohamad Sadeghi, *Environ. Prog. Sustainable Energy*, 2023, **42**, e13954.
- 29 R. Ou, H. Zhang, V. X. Truong, L. Zhang, H. M. Hegab, L. Han, J. Hou, X. Zhang, A. Deletic and L. Jiang, *Nat Sustainability*, 2020, **3**, 1052–1058.
- 30 M. Wang, S. Zhou, S. Cao, Z. Wang, S. Liu, S. Wei, Y. Chen and X. Lu, *J. Mater. Chem. A*, 2020, **8**, 10519–10533.
- 31 J. Park, D. Yuan, K. T. Pham, J.-R. Li, A. Yakovenko and H.-C. Zhou, *J. Am. Chem. Soc.*, 2012, **134**, 99–102.
- 32 Y. Jiang, P. Tan, S. C. Qi, X. Q. Liu, J. H. Yan, F. Fan and L. B. Sun, *Angew. Chem., Int. Ed.*, 2019, **58**, 6600–6604.
- 33 Y. Zhu and W. Zhang, *Chem. Sci.*, 2014, **5**, 4957–4961.
- 34 H. Li, M. R. Hill, C. Doblin, S. Lim, A. J. Hill and P. Falcaro, *Adv. Funct. Mater.*, 2016, **26**, 4815–4821.



- 35 K. Matsuda and M. Irie, *J. Photochem. Photobiol., C*, 2004, **5**, 169–182.
- 36 R. Lyndon, K. Konstas, R. A. Evans, D. J. Keddie, M. R. Hill and B. P. Ladewig, *Adv. Funct. Mater.*, 2015, **25**, 4405–4411.
- 37 A. Liu, C. Mollart, A. Trewin, X. Fan and C. H. Lau, *ChemSusChem*, 2023, e202300019.
- 38 C. R. Crecca and A. E. Roitberg, *J. Phys. Chem. A*, 2006, **110**, 8188–8203.
- 39 K. Tsuda, G. C. Dol, T. Gensch, J. Hofkens, L. Latterini, J. W. Weener, E. W. Meijer and D. Schryver, *J. Am. Chem. Soc.*, 2000, **122**, 3445–3452.
- 40 G. Hartley and R. Le Fevre, *J. Chem. Soc.*, 1939, 531–535.
- 41 X. Dong, A. Akram, B. Comesaña-Gándara, X. Dong, Q. Ge, K. Wang, S.-P. Sun, B. Jin and C. H. Lau, *ACS Appl. Polym. Mater.*, 2020, **2**, 2586–2593.
- 42 C. Graham, J. Pierrus and R. Raab, *Mol. Phys.*, 1989, **67**, 939–955.
- 43 S. Saqib, S. Rafiq, N. Muhammad, A. L. Khan, A. Mukhtar, N. B. Mellon, Z. Man, M. H. Nawaz, F. Jamil and N. M. Ahmad, *J. Nat. Gas Sci. Eng.*, 2020, **73**, 103072.
- 44 L. A. Neves, J. G. Crespo and I. M. Coelho, *J. Membr. Sci.*, 2010, **357**, 160–170.
- 45 J. W. To, J. He, J. Mei, R. Haghighpanah, Z. Chen, T. Kurosawa, S. Chen, W.-G. Bae, L. Pan and J. B.-H. Tok, *J. Am. Chem. Soc.*, 2016, **138**, 1001–1009.
- 46 S. Mane, Z.-Y. Gao, Y.-X. Li, D.-M. Xue, X.-Q. Liu and L.-B. Sun, *J. Mater. Chem. A*, 2017, **5**, 23310–23318.
- 47 H. Margenau, *Rev. Mod. Phys.*, 1939, **11**, 1.
- 48 J. Law, M. Van Baalen, M. Foy, S. S. Mason, C. Mendez, M. L. Wear, V. E. Meyers and D. Alexander, *J. Occup. Environ. Med.*, 2014, **56**, 477–483.
- 49 B. P. Spigarelli and S. K. Kawatra, *J. CO₂ Util.*, 2013, **1**, 69–87.
- 50 M. L. Chua, L. Shao, B. T. Low, Y. Xiao and T.-S. Chung, *J. Membr. Sci.*, 2011, **385**, 40–48.
- 51 J. Liu, J. Tian, P. K. Thallapally and B. P. McGrail, *J. Phys. Chem. C*, 2012, **116**, 9575–9581.
- 52 Y. Zhao, K. X. Yao, B. Teng, T. Zhang and Y. Han, *Energy Environ. Sci.*, 2013, **6**, 3684–3692.
- 53 Y. Cui, Y. Xing, J. Tian, W. Su, F.-Z. Sun and Y. Liu, *Fuel*, 2023, **337**, 127179.
- 54 F. Raganati, M. Alfe, V. Gargiulo, R. Chirone and P. Ammendola, *Chem. Eng. J.*, 2019, **372**, 526–535.
- 55 S. Lagergren, *K. Sven. Vetenskapsakad. Handl.*, 1898, **24**, 1–39.
- 56 S. Loganathan, M. Tikmani, S. Edubilli, A. Mishra and A. K. Ghoshal, *Chem. Eng. J.*, 2014, **256**, 1–8.
- 57 S. Mutyala, M. Jonnalagadda, H. Mitta and R. Gundaboyina, *Chem. Eng. Res. Des.*, 2019, **143**, 241–248.
- 58 Y.-S. Ho and G. McKay, *Process Biochem.*, 1999, **34**, 451–465.
- 59 B. Guo, Y. Wang, X. Qiao, X. Shen, J. Guo, J. Xiang and Y. Jin, *Chem. Eng. J.*, 2021, **421**, 127865.
- 60 X. Wang, L. Chen and Q. Guo, *Chem. Eng. J.*, 2015, **260**, 573–581.
- 61 Y. Liu and X. Yu, *Appl. Energy*, 2018, **211**, 1080–1088.
- 62 Q. Liu, J. Shi, S. Zheng, M. Tao, Y. He and Y. Shi, *Ind. Eng. Chem. Res.*, 2014, **53**, 11677–11683.
- 63 N. J. Nagelkerke, *Biometrika*, 1991, **78**, 691–692.
- 64 L. Shao, Y. Sang, J. Huang and Y.-N. Liu, *Chem. Eng. J.*, 2018, **353**, 1–14.
- 65 M. Liu, L. Shao, J. Huang and Y.-N. Liu, *Microporous Mesoporous Mater.*, 2018, **264**, 104–111.
- 66 F. Raganati, R. Chirone and P. Ammendola, *Ind. Eng. Chem. Res.*, 2020, **59**, 3593–3605.
- 67 T. Takagishi, A. Katayama, M. Matsuoka, K. Konishi and N. Kuroki, *Kolloid-Zeitschrift und Zeitschrift für Polymere*, 1969, **232**, 699–703.
- 68 H. Gilman and R. M. Pickens, *J. Am. Chem. Soc.*, 1925, **47**, 2406–2416.
- 69 R. G. Denning and J. Thatcher, *J. Am. Chem. Soc.*, 1968, **90**, 5917–5918.
- 70 A. Basile, A. Gugliuzza, A. Iulianelli and P. Morrone, in *Advanced Membrane Science and Technology for Sustainable Energy and Environmental Applications*, Elsevier, 2011, pp. 113–159.
- 71 *Average Cost Of Electricity Per KWh (UK 2023 Updated)*, <https://energyguide.org.uk/average-cost-electricity-kwh-uk/>.

